small NANO MICRO

Graphene

How Does Graphene Grow? Easy Access to Well-Ordered Graphene Films

Frank Müller, Hermann Sachdev, Stefan Hüfner, Andrew J. Pollard, Edward W. Perkins, James C. Russell, Peter H. Beton, Stefan Gsell, Martin Fischer, Matthias Schreck, and Bernd Stritzker*

The selective formation of large-scale graphene layers on a Rh-YSZ-Si(111) multilayer substrate by a surface-induced chemical growth mechanism is investigated using low-energy electron diffraction, X-ray photoelectron spectroscopy, X-ray photoelectron diffraction, and scanning tunneling microscopy. It is shown that well-ordered graphene layers can be grown using simple and controllable procedures. In addition, temperature-dependent experiments provide insight into the details of the growth mechanisms. A comparison of different precursors shows that a mobile dicarbon species (e.g., C_2H_2 or C_2) acts as a common intermediate for graphene formation. These new approaches offer scalable methods for the large-scale production of high-quality graphene layers on silicon-based multilayer substrates.

Keywords:
- epitaxy
- graphene
- monolayers
- self-assembly
- surface analysis

[*] Dr. H. Sachdev, Dr. F. Müller
Anorganische und Allgemeine Chemie FR 8.1
Naturwissenschaftlich-Technische Fakultät III
Chemie,
Pharmazie und Werkstoffwissenschaften
Universität des Saarlandes C4.1
66041 Saarbrücken (Germany)
E-mail: h.sachdev@mx.uni-saarland.de

Dr. F. Müller, Prof. S. Hüfner
Institut für Experimentalphysik
Naturwissenschaftlich-Technische Fakultät II
Physik und
Mechatronik
Universität des Saarlandes
66041 Saarbrücken (Germany)

A. J. Pollard, Dr. E. W. Perkins, J. C. Russell, Prof. P. H. Beton
School of Physics and Astronomy, University of Nottingham
University Park, Nottingham, NG7 2RD (UK)

Dr. S. Gsell, M. Fischer, Dr. M. Schreck, Prof. B. Stritzker
Institut für Physik, Lehrstuhl für Experimentalphysik IV
Universität Augsburg
Universitätsstaße 1
86135 Augsburg (Germany)

Supporting Information is available on the WWW under http://www.small-journal.com or from the author.

DOI: 10.1002/smll.200900158

1. Introduction

Graphite had its first strong impact on information technology in the 18th century when the quill was replaced by the pencil. Now, nearly three centuries later, attention is focused on graphene, a 2D network of carbon atoms arranged in a honeycomb-type structure and also an individual building block of the graphite structure, as a potential successor to silicon as the preferred material for the active region of nanostructured electronic devices.[1–5] A graphene sheet is formed from a hexagonal honeycomb-like array of threefold coordinated carbon atoms with a thickness of only one monolayer. Graphene nanosheets extracted from chemical solutions or by using exfoliation have demonstrated the great promise of this material for nanoscale engineering and the fabrication of nanoscale electronic devices.[6,7] However, for many applications it is desirable to avoid corrugations and control the orientation of graphene over large areas, providing strong motivation for epitaxial growth of graphene on a substrate crystal.[2]

For the preparation of graphene-based materials, high-quality graphene sheets consisting of a monolayer of carbon atoms have to be generated in large quantities, and an ideal method should also be selective regarding monolayer or

multilayer graphene growth. Regarding the current methods for the preparation of graphene layers such as mechanical or chemical cleavage of graphite,[4,8,9] bottom-up approaches by chemical synthesis,[10] and epitaxial growth methods on silicon carbide[2,11] or on metal substrates,[12–14] these individual approaches have to be considered with respect to the resulting graphene sheet size and quality, since in some cases graphene multilayer formation may also occur. A common aspect of the experiments reported so far is that the graphene layers are prepared using methods based on high-cost instruments or with limited scope for scalable mass production.

In another recent study, the growth of graphene on Ru(0001) was controlled by the temperature-dependent carbon solubility within the substrate lattice.[12] This procedure resulted in graphene layers of very high quality, although the origin of the carbon was not discussed. In addition, most experiments reported so far are focused primarily on the production of well-ordered graphene layers rather than the mechanism of growth. Thus, there is still little information why a particular recipe works while another one fails. The goal of the present study is firstly to present alternative procedures for the growth of well-ordered graphene layers that are well-suited to mass production at low cost. Secondly, the growth chemistry is investigated and a mechanism is proposed.

2. Results and Discussion

Here we show the formation of graphene layers by controlled degradation of acetaldehyde ($H_3C-C(O)H$) and acetone ($H_3C-C(O)-CH_3$). We consider first the use of acetaldehyde as a precursor for ex situ dosing of the substrate. A clean Rh-YSZ-Si(111) surface (150-nm Rh on a 25-nm yttria-stabilized zirconia (YSZ) buffer layer on Si(111)) without any C- and O-impurities according to X-ray photoelectron spectroscopy (XPS) (approximate dimensions 1 cm × 1 cm, prepared as described in Supporting Information) is rinsed in acetaldehyde. Rh-YSZ-Si(111) substrates represent a low-cost alternative to a Rh(111) single crystal and are already available on 4-in. wafers.[15,16] After the initial rinsing, the sample is transferred to a vacuum system (base pressure $\approx 10^{-10}$ mbar) and investigated using low-energy electron diffraction (LEED) and XPS. Immediately after introduction to the vacuum system the surface is completely disordered (as observed by LEED), but in Figure 1, the XPS data display exactly the expected 2:1 carbon-to-oxygen ratio, as expected for the stoichiometry of the precursor. After applying a controlled thermal ramping up to 1 000 K in situ (for details, see Supporting Information), the oxygen intensity in XPS drops below the detection limit (Figure 1).

The mean thickness $\langle d \rangle$ of the remaining carbon species corresponds to approximately one monolayer. This value is estimated from the angular distribution of the photoelectron intensity leading to a value of $\langle d \rangle = 0.25\,\lambda$ (Figure 2a). The electron mean free path, λ, is ≈1 nm for the electron energies used here. Therefore, $\langle d \rangle$ is ≈75% of the interlayer spacing of graphite along the c-axis (≈335 pm[17]) or approximately one monolayer. Since the damping of the substrate intensities is just a measure for the mean thickness of the carbon film, the same value of $\langle d \rangle$ could, in principle, also arise from a partial

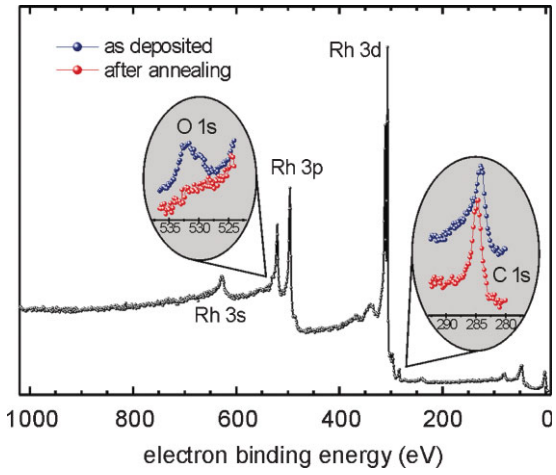

Figure 1. XPS spectra (AlKα, $\hbar\omega = 1\,486.6$ eV) of a Rh-YSZ-Si(111) substrate after ex situ deposition of acetaldehyde. The survey spectrum (black) refers to the sample after annealing up to 1 000 K. The detailed spectra display the relative amount of carbon and oxygen before (blue) and after annealing (red).

coverage by multilayer domains. In X-ray photoelectron diffraction (XPD), the angular distribution of the C1s photoelectron intensity may be used to rule out this explanation. Briefly, in XPD, the forward scattering of the electron waves by regions of a crystalline solid between the emitting atom and the surface of the solid leads to an anisotropy in the angular distribution of the photoelectron intensity. An absence of anisotropy indicates that the emitting atom is located

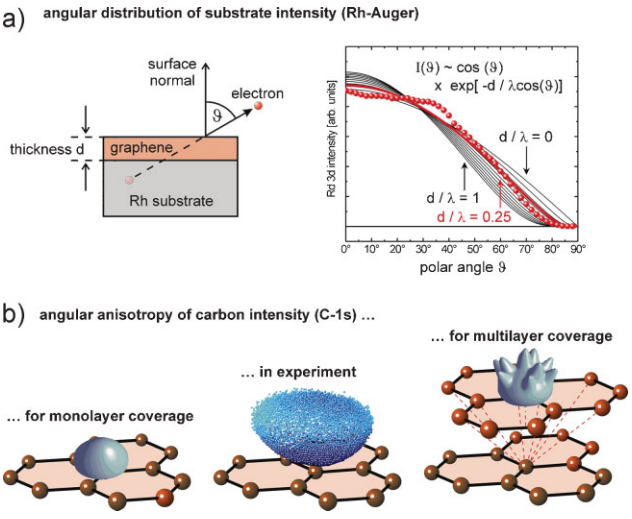

Figure 2. a) Estimation of the mean thickness of a carbon film via the polar photoelectron intensity distribution of the Rh-MVV-Auger electrons with E_{kin} ≈300 eV (with M and V describing the shells of the Auger process). Although the impact of forward scattering is reduced by the low kinetic energy, by the azimuthally averaging of the data, and by the use of full apertures, the red experimental data still display a slight modulation by forward scattering. The mean thickness of the carbon coverage is typically 25% of the electron mean free path, or 0.2–0.3 nm, corresponding to about 1 monolayer. b) The nearly homogeneous distribution of the C1s photoelectron intensity in XPD with no forward scattering maxima displays the characteristics of full monolayer coverage rather than of partial coverage by multilayer domains.

NANO MICRO small

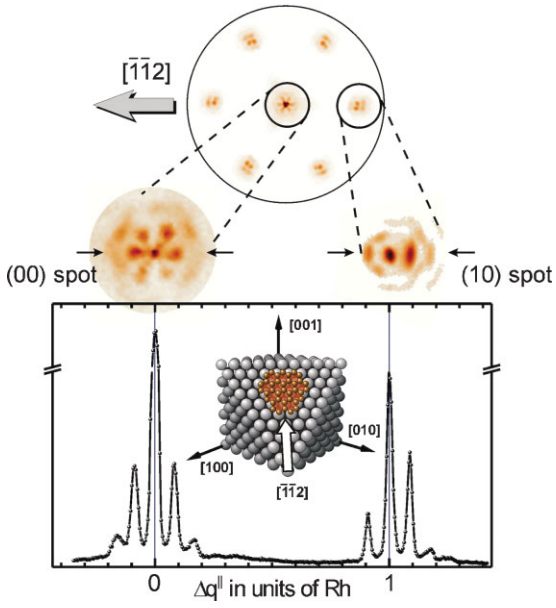

Figure 3. LEED pattern and polar intensity plot ($E_0 = 45$ eV) along the $[\bar{1}\,\bar{1}2]$ symmetry axis for an in situ cleaned Rh-YSZ-Si(111) surface after ex situ preparation by acetaldehyde. The additional non-integral intensity contributions around the (00) and (10) spots indicate the formation of a well-ordered superstructure.

exclusively at the topmost layer. No forward scattering modulations of the C1s intensity are observed (Figure 2b), confirming that the carbon forms a monolayer film rather than multilayer domains.

Investigation of the sample using LEED reveals distinct spots as shown in Figure 3. Qualitatively, the high crystalline order of the carbon film is illustrated by the additional intensity peaks around the principal spots of the substrate. These additional peaks are attributed to a $(m \times m)/(n \times n)$ superstructure with nearly perfect six-fold symmetry, where m and n are the numbers of the primitive unit cells of the epitaxial layer and the substrate, respectively. Quantitatively, the analysis of the polar intensity distributions of the (00) and (10) spots along the $[\bar{1}\,\bar{1}2]$ [symmetry axis results in a superstructure of approximately (12×12) graphene on (11×11) Rh(111) unit cells consistent with the near equality ($\delta \approx 0.2\%$) of $11 \times a_{111}[\mathrm{Rh}] = 2\,959$ pm and $12 \times a[\mathrm{graphene}] = 2\,952$ pm ($a_{111}[\mathrm{Rh}] \approx 269$ pm[18] versus $a[\mathrm{graphene}] \approx 246$ pm[17]). A similar superstructure is observed when boron nitride is deposited on Rh(111).[19–23] Our results show clearly that (at least on a Rh(111) surface) the deposited carbon species strongly tend toward self-organization: although the overall growth mechanism starts with an uncontrolled deposition of an undefined amount of carbon-containing species, the decomposition of the precursor as well as the reorganization of the remaining carbon species finally result in the formation of a well-ordered graphene sheet with a thickness of approximately one monolayer.

The formation of graphene monolayers is not restricted to the use of acetaldehyde as a precursor, and there are a large variety of synthetic and natural carbon compounds offering similar decomposition routes (Figure 4). We also highlight the nonspecific requirement of the carbon source through, for example, the formation of graphene due to contamination from sample handling (a fingerprint), which is described in detail in the Supporting Information. Moreover, we focus on the possibility that carbon feedstock may be inadvertently introduced through procedures such as sample cleaning. In surface science, the pretreatment of a sample usually starts with an ex situ cleaning, for example, by organic solvents such as acetone, ethanol, propanol, etc., which also represent carbon sources. In order to demonstrate the impact of such a process, an atomically clean Rh-YSZ-Si(111) surface (as prepared in situ by, for example, Ar ion etching with no oxygen or carbon contaminations detected in XPS) was exposed to ambient conditions for several days and washed with acetone for a few seconds. If such a sample is annealed in ultrahigh vacuum (UHV) ($\approx 5 \times 10^{-10}$ mbar; temperature slowly increased to 1 000 K, for details see Supporting Information), the surface then displays all the characteristics of a well-ordered graphene

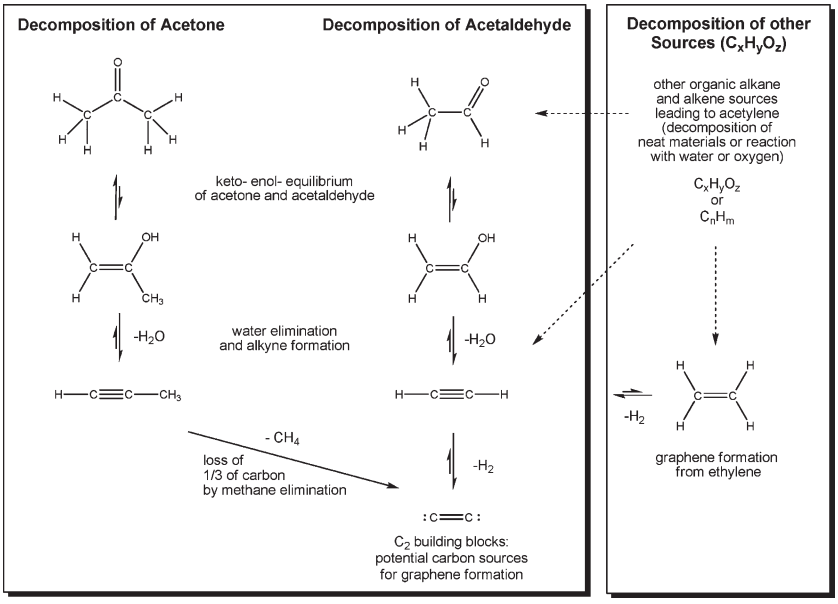

Figure 4. Summary of the gross chemical reactions involved for the graphene film formation from acetone (left), acetaldehyde (middle), and a general $C_xH_yO_z$ precursor (right). For acetaldehyde and acetone, the reactions involving the keto–enol tautomerism are shown. In both cases, water elimination from the enol form leads to an alkyne intermediate (acetylene from acetaldehyde and propyne from acetone). Further elimination of methane in the latter system explains the loss of one third of the total carbon amount in Figure 7, leading to acetylene and finally C_2 acting as growth species while being templated on the transition metal surface. Furthermore, an alternative route to graphene via an acetylene intermediate starting from ethylene or ethane by transition-metal-catalyzed dehydrogenation reaction is denoted in the left part, as reported in Reference [13]. This schematic representation reveals a generalized insight into the mechanisms involved in graphene formation from molecular precursors enabling a facile formation of high-quality graphene layers, as presented in this study.

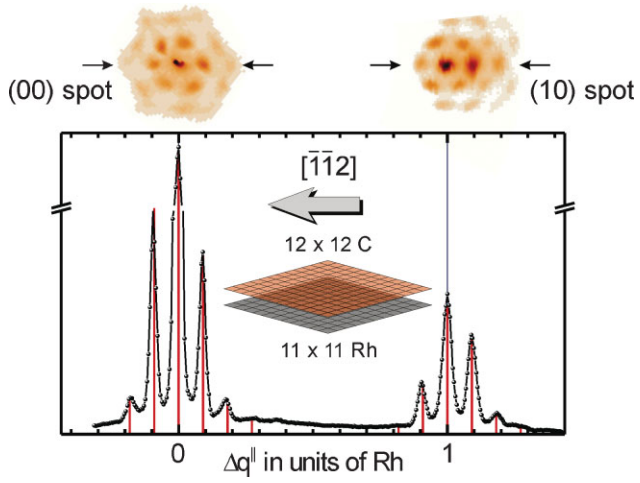

Figure 5. a) LEED polar intensity plot ($E_0 = 45$ eV) along the [$\bar{1}\,\bar{1}$2] symmetry axis for an in situ-cleaned Rh-YSZ-Si(111) surface after 5 days air exposure, followed by acetone washing and subsequent annealing in UHV ($\approx 5 \times 10^{-10}$ mbar) up to 1 000 K. The additional non-integral intensity contributions around the (00) and (10) spots appear up to the third order and are equidistantly distributed, indicating a nearly perfect commensurate (12 × 12)/(11 × 11) superstructure, as depicted by the red lines.

monolayer, as characterized by the LEED data in Figure 5. The nearly perfect structural quality is further verified by the superstructure spots that appear up to the third order. In addition to these data from reciprocal space, a high degree of ordering is also verified in real space by ex situ STM images of the sample, which clearly reveal a full coverage of the substrate with the graphene superstructure (Figure 6). The periodic structure in Figure 6 arises from a Moiré pattern, similar to that

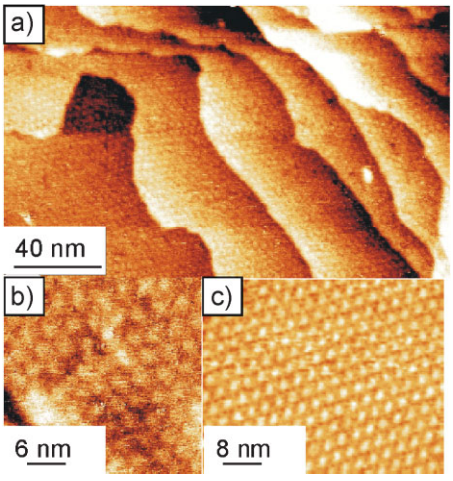

Figure 6. a) STM image of graphene formed by exposing a Rh(111) thin film to atmosphere for several days followed by dipping in acetone and subsequent annealing in vacuum. Following graphene formation the sample was stored and imaged under ambient conditions (scanning parameters: sample voltage 0.1V, tunnel current 1 nA). b) Higher-magnification STM image of the surface (0.07 V, 1 nA) under ambient conditions. c) STM image (1.0 V, 0.2 nA) of graphene layer acquired in situ immediately after the annealing cycle described in paper. In all images the periodic structure (period ≈3 nm) arises from a Moiré pattern due to the superstructure of the graphene layer as described in the text.

previously observed for graphene on iridium and boron nitride on rhodium[13,14] and confirms the formation of the superstructure described above. Since these STM data were recorded from a sample that had been transferred to another UHV system through ambient conditions, Figure 6 also demonstrates the stability of the graphene layer, which will be of importance for the use as a substrate for other systems.

From our results it is clear that great care must be taken when investigating the formation of a graphene layer by a particular in situ procedure and, in particular, our results highlight the possibility that graphene formation can be influenced, or even controlled, by ex situ pretreatment of the surface. When the above test is slightly modified so that clean a Rh-YSZ-Si(111) surface (without long-term air exposure) is rinsed in acetone (following the methodology for acetaldehyde dosing), the formation of a graphene monolayer is also clearly observed. Thus, acetone can also serve as a single-source precursor for the preparation of graphene layers.

For the acetone-derived graphene we have acquired LEED and XPS data at several temperatures as shown in Figure 7. These data provide detailed information about the chemistry of the growth mechanism of graphene films. After dipping a clean sample (without C– and O– impurities according to XPS) in acetone for approximately 1 min at 300 K, the LEED polar intensity plots show a disordered surface with a carbon-to-oxygen ratio (inferred from XPS) close to the 3:1 ratio of the precursor (C_3H_6O). The sample is then annealed at about 400–450 K for several hours, after which the XPS data show a near complete removal of oxygen as well as a reduction in the amount of carbon by about a third. These data suggest that there is a (stepwise) decomposition of the precursor on the surface. The oxygen peak drops below the detection limit and the carbon intensity nearly remains constant (at least within the error bar of XPS) while the sample is annealed at 700 K. In this temperature range we observe the onset of graphene formation, which is indicated by the onset of the superstructure spots in LEED. The observation of diffuse, but clearly visible graphene-related superstructure spots within the corresponding LEED profile indicates that an agglomeration of the remaining carbon species to small domains takes place. Finally, when the temperature is increased to about 1 000 K, domain growth takes place, resulting in the observation of distinct, sharp superstructure spots within the LEED profile. Figure 6b shows an STM image of a sample that was acquired in situ following the preparation of a sample following the above thermal cycle. The image confirms that there is a near complete coverage of the surface with a graphene superstructure and its associated Moiré pattern, similar to that observed previously for graphene on iridium and boron nitride on rhodium.[13,14]

We interpret this set of data as follows. The XPS results are consistent with a first stage of elimination of water (from the enolate form of acetone, see also Supporting Information), followed or accompanied by the elimination of methane (loss of one third of the total carbon) to form acetylene templated on the metal surface. In our studies of the acetone decomposition the loss of oxygen in a temperature range up to 450 K is an important finding because this type of deoxygenation reaction is only compatible with a dehydration mechanism (loss of H_2O), since a loss of oxygen through a direct cleavage of the

NANO MICRO small

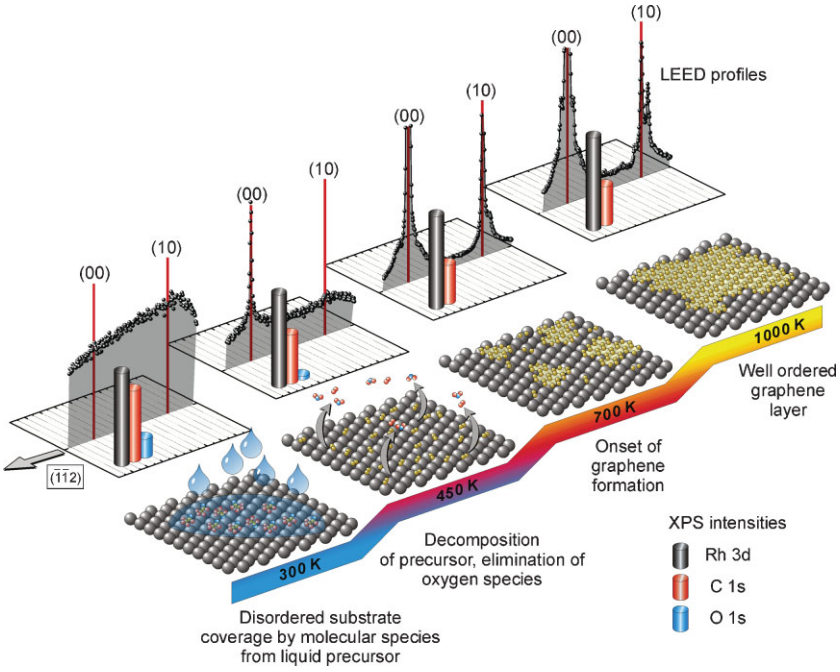

Figure 7. Temperature-dependence of the graphene formation for a clean Rh-YSZ-Si(111) surface that was dipped in acetone for about 60 s. At 300 K, the initial disordered surface displays nearly the nominal carbon-to-oxygen ratio (3:1) of the precursor. The decomposition of the precursor starts in the range of about 450 K while the onset of the graphene formation can be observed in the range of about 700 K. In the temperature range at about 1 000 K, the small graphene domains finally agglomerate to larger ones.

C=O double bond is chemically not feasible under the applied conditions (for further details concerning the chemistry of the growth mechanism, see Supporting Information).

Since the resulting graphene film of considerable high quality is grown from mobile species on the surface and considering the precursor chemistry, we propose the following gross decomposition route. The precursor can eliminate water and methane, followed by the desorption of hydrogen during higher temperature annealing, and finally resulting in mobile and reactive C_2 species as the actual growth species for graphene. These findings are fundamental for the understanding of graphene growth and according to this decay mechanism, other precursors that follow a decomposition route resulting in C_2 can be considered as suitable candidates for graphene precursors, as initially demonstrated by the data obtained from acetaldehyde, C_2H_4O. This interpretation is also in accordance with a simulation of the decay of acetaldehyde.[24] Figure 4 summarizes the proposed decay mechanisms for acetone and acetaldehyde, indicating that graphene formation is achieved by reactions finally leading to common intermediates, namely C_2 units, irrespective of the starting materials. Furthermore, this interpretation is also in accordance with the formation of graphene from ethylene,[13,14] since transition metals catalyze dehydrogenation reactions.

3. Conclusion

In this report it is demonstrated by the decay of acetone and acetaldehyde that the buildup of graphene layers may be regarded as a mechanism involving C_2 units as dominant growth species on the substrate finally formed from the decay of molecular precursors. Our results also contribute to a general understanding of the transition-metal-templated carbon formation within the C–H–O system. The scalable approach of graphene formation reported here provides an important route to the mass production of epitaxial graphene monolayers on silicon-based multilayer substrates, which are already available in 4-in. wafers.[15,16] Regarding future applications, selectively grown graphene monolayers on wide band-gap materials like silicon carbide single crystals or boron nitride monolayers on metal substrates[19–23] or even oxides may certainly be of interest for the development of new nanoscale electronic devices, and the procedures presented here as well as chemical vapor deposition (CVD) growth from the gas phase with these precursor systems will open a new research field for selective graphene growth.

4. Experimental Section

The Rh-YSZ-Si(111) substrates were prepared as described in Reference [15]. The experiments were performed with an ESCA Mk II spectrometer by Vacuum Generators. The XPS and XPD data were recorded with AlKα radiation at 1 486.6 eV (in normal emission mode for XPS). For the hemispherical LEED patterns and polar intensity plots, the angular part of the setup was operated in the XPD mode while the spectroscopic part was operated in the elastic EELS mode, that is, the intensity of the elastically scattered electrons at $\Delta E = 0$ were recorded for the variation of the angular setting (ϑ,φ). The experimental setup is described in detail in References [25, 26].

The initial Rh-YSZ-Si(111) substrates were cleaned by several cycles of Ar ion etching and subsequent annealing at 1 000 K until the C1s and O1s intensities were beyond the detection limit. Throughout the later experiments, the graphene layer of a preceding experiment could be easily removed by applying 10 L oxygen at about 1 000 K, leaving a clean Rh surface of perfect (111) order. After the ex situ rinsing of the substrate by acetone or acetaldehyde, the in situ ramping of the temperature started with 400–450 K for about 12 h, followed by an increase of the temperature in steps of 100 K up to about 1 000 K with each temperature applied for about 2 h.

Acknowledgements

This work was supported by the European Union under Contract No. NMP4-CT-2004-013817 [Specific Targeted Research Project

"Nanomesh"]. The Nottingham authors also acknowledge financial support from the UK Engineering and Physical Science Research Council under projects EP/C534158/1 and EP/D048761/1.

[1] K. S. Novoselov, A. K. Geim, S. V. Morozov, D. Jiang, Y. Zhang, S. V. Dubonos, I. V. Grigorieva, A. A. Firsov, *Science* **2004**, *306*, 666.
[2] C. Berger, Z. Song, X. Li, X. Wu, N. Brown, C. Naud, D. Mayou, T. B. Li, J. Hass, A. N. Marchenkov, E. H. Conrad, P. N. First, W. A. de Heer, *Science* **2006**, *312*, 1191.
[3] L. A. Ponomarenko, F. Schedin, M. I. Katsnelson, R. Yang, E. W. Hill, K. S. Novoselov, A. K. Geim, *Science* **2008**, *320*, 356.
[4] A. K. Geim, K. S. Novoselov, *Nat. Mater.* **2007**, *6*, 183.
[5] P. Avouris, J. Chen, *Mater. Today* **2006**, *9*, 46.
[6] D. Li, B. Kaner, *Science* **2008**, *320*, 1170.
[7] J. S. Bunch, A. M. van der Zande, S. S. Verbridge, I. W. Frank, D. M. Tanenbaum, J. M. Parpia, H. G. Craighead, P. L. McEuen, *Science* **2007**, *315*, 490.
[8] M. J. McAllister, J.-L. Li, D. H. Adamson, H. C. Schniepp, A. A. Abdala, J. Liu, M. Herrera-Alonso, D. L. Milius, R. Car, R. K. Prud'homme, I. A. Aksay, *Chem. Mater.* **2007**, *19*, 4396.
[9] S. Stankovich, D. A. Dikin, R. D. Piner, K. A. Kohlhaas, A. Kleinhammes, Y. Jia, Y. Wu, S. T. Nguyen, R. S. Ruoff, *Carbon* **2007**, *45*, 1558.
[10] J. S. Wu, W. Pisula, K. Müllen, *Chem. Rev.* **2007**, *107*, 718.
[11] M. L. Sadowski, G. Martinez, M. Potemski, C. Berger, W. A. de Heer, *Solid State Commun.* **2007**, *143*, 123.
[12] P. W. Sutter, J. I. Flege, E. A. Sutter, *Nat. Mater.* **2008**, *7*, 406.
[13] A. T. N'Diaye, S. Bleikamp, P. J. Feibelman, T. Michely, *Phys. Rev. Lett.* **2006**, *97*, 215501.
[14] D. Martoccia, P. R. Willmott, T. Brugger, M. Björck, S. Günther, C. M. Schlepütz, A. Cervellino, S. A. Pauli, B. D. Patterson, S. Marchini, J. Wintterlin, W. Moritz, T. Greber, *Phys. Rev. Lett.* **2008**, *101*, 126102.
[15] S. Gsell, PhD Thesis, Augsburg University 2008.
[16] S. Gsell, M. Fischer, R. Brescia, M. Schreck, P. Huber, F. Bayer, B. Stritzker, D. G. Schlom, *Appl. Phys. Lett.* **2007**, *91*, 061501.
[17] G. E. Bacon, *Acta Crystallogr.* **1951**, *4*, 558.
[18] H. P. Singh, *Acta Crystallogr.* **1968**, *A24*, 469.
[19] M. Corso, W. Auwärter, M. Muntwiler, A. Tamai, T. Greber, J. Osterwalder, *Science* **2004**, *303*, 217.
[20] F. Müller, S. Hüfner, H. Sachdev, *Surf. Sci.* **2009**, *603*, 425.
[21] S. Berner, M. Corso, R. Widmer, O. Groening, R. Laskowski, P. Blaha, K. Schwarz, A. Goriachko, H. Over, S. Gsell, M. Schreck, H. Sachdev, T. Greber, J. Osterwalder, *Angew. Chem.* **2007**, *46*, 5115.
[22] R. Laskowski, P. Blaha, T. Gallauner, K. Schwarz, *Phys. Rev. Lett.* **2007**, *98*, 106802.
[23] R. Laskowski, P. Blaha, *J. Phys. Condens. Matter* **2008**, *20*, 064207.
[24] X. Yang, S. Maeda, K. Ohno, *J. Phys. Chem. A* **2007**, *111*, 5099.
[25] F. Müller, K. Stöwe, H. Sachdev, *Chem. Mater.* **2005**, *17*, 3464.
[26] F. Müller, R. de Masi, D. Reinicke, P. Steiner, S. Hüfner, K. Stöwe, *Surf. Sci.* **2002**, *520*, 158.

Received: January 28, 2009
Revised: May 15, 2009
Published online: June 29, 2009

